scientific reports

Check for updates

OPEN

Dipolar modulation of surface states in GaN via molecular ionization energy

Or Haim Chaulker[1], Yury Turkulets[2], Yoram Shapira[3], R. S. Goldman[2] & Ilan Shalish[1]✉

Gallium nitride (GaN) surface states play a pivotal role in determining device performance and stability. Here, we show that adsorption of molecules with varying ionization energies modulates GaN surface states, as revealed by surface photovoltage and X-ray photoelectron spectroscopy. We find a linear relationship between adsorbate ionization energy and surface Fermi level, indicating that the Ga-polar surface is not intrinsically pinned but is tunable via charge transfer at the native oxide interface. Removal of this oxide suppresses molecular effects, confirming the active state at the GaN/native oxide interface. The low work function values of adsorbed layers suggest robust, ambient-stable dipolar structures, offering a possible new route for negative electron affinity (NEA) activation. Our findings provide a framework for targeted GaN surface engineering in electronic devices.

Surface states in GaN critically affect the performance of high-frequency and high-power devices such as high electron mobility transistors (HEMTs) and metal-oxide-semiconductor field-effect transistors (MOSFETs)[1–3]. Located at, or near, the Ga-face of c-plane GaN, these states contribute to phenomena such as current collapse, threshold voltage instability, and gate leakage[4–7]. Unlike silicon, GaN lacks a high-quality native oxide, making its surface highly reactive and sensitive to environmental adsorbates[8–10]. This study explores how molecular adsorption modulates surface charge and Fermi level alignment, offering insights into surface passivation strategies.

Recent advances have highlighted the role of ambient molecules in modulating GaN surface charge. Adsorption of air constituents such as NO_2, CO, and H_2O has been shown to induce significant changes in surface potential and charge distribution[11–14]. In our previous work[14], we demonstrated that selective adsorption of NO_2 on the Ga-face of c-plane GaN leads to reproducible changes in surface charge density, as revealed by surface photovoltage spectroscopy (SPS) and photoluminescence (PL). These findings suggest that the yellow-luminescence-associated surface state is populated by external charge carriers originating from adsorbed molecules, and that this state is chemically sensitive to NO_2 exposure.

Building on these insights, the present study investigates the relationship between the ionization energy of adsorbed molecules and the position of the surface Fermi level relative to the conduction band. By assuming equivalence between surface charge density and molecular coverage, we demonstrate a linear dependence of Fermi level position on molecular ionization energy. At face value, this behavior suggests that the Ga-polar-face of GaN is not pinned by surface states, and the Fermi level is thus free to assume a different position for different adsorbates. Our analysis reveals that the observed Fermi level modulation is consistent with native-oxide-mediated charge transfer.

A key new observation is that the surface charge density distribution peaks—previously attributed to molecular adsorption—are only present when the native oxide remains intact. Upon oxide removal, these features vanish, suggesting that the surface state responsible for charge trapping is not intrinsic to the GaN bulk but rather emerges at the GaN/native oxide interface. This finding challenges conventional assumptions about bulk-dominated surface states and points to the oxide-semiconductor interface as the locus of electronic activity[15–18].

The nature of native oxides on GaN has been explored in several studies, revealing that Ga_2O_3-like phases form spontaneously under ambient conditions and exhibit distinct electronic and structural properties[19–22]. These oxides have been shown to influence surface wettability, chemical reactivity, and electronic band alignment[23,24]. Moreover, their interaction with adsorbed molecules can lead to complex dipolar and charge-transfer phenomena, further modulating the surface electronic structure[25–27].

[1]School of Electrical and Computer Engineering, Ben Gurion University of the Negev, 8410501 Beer Sheva, Israel. [2]Department of Materials Science and Engineering, University of Michigan, Ann Arbor, MI 48109, USA. [3]School of Electrical Engineering, Tel Aviv University, 6997801 Tel Aviv, Israel. ✉email: shalish@bgu.ac.il

By integrating experimental data with electrostatic modeling, this work provides a new perspective on the origin and tunability of surface states in GaN. It opens pathways for targeted surface engineering and passivation strategies that leverage molecular dipole interactions and oxide interface control[28–30]. Our findings also contribute to the broader understanding of Fermi level pinning, interface dipoles, and molecule-semiconductor coupling—topics of growing importance in both inorganic and organic electronics[31–35].

Materials and methods

A 2.2 µm-thick GaN epilayer, grown by metal–organic chemical vapor deposition (MOCVD) on c-plane sapphire, was utilized for this study. The sample had a Ga-face orientation and was co-doped with silicon and magnesium. While Mg doping partially compensated the n-type behavior induced by Si, the layer retained net n-type conductivity, exhibiting a carrier concentration of approximately $2 \cdot 10^{16} cm^{-3}$ as determined by Hall effect measurements.

Surface photovoltage spectroscopy (SPS) was conducted using a Kelvin Probe system (Besocke Delta Phi GmbH). Illumination was provided by a 300 W xenon short-arc lamp, with monochromatization achieved through a Newport MS257 spectrometer and long-pass order-sorting filters. A computer-controlled slit system ensured a constant photon flux across the full spectral range. For each photon energy increment, the sample was illuminated for 5 minutes before measuring the contact potential difference (CPD). Prior to data acquisition, the sample was allowed to return to equilibrium in darkness over a period of at least 48 hours.

All the photovoltage measurements were carried out within a grounded stainless-steel chamber. Depending on the specific measurement, the chamber was either maintained under high vacuum (base pressure below $1 \cdot 10^{-5} mbar$ or evacuated and subsequently filled with selected gases at atmospheric pressure. The samples were mounted on a temperature-controlled stage, stabilized at 305 K throughout the measurements.

Surface charge density spectra were calculated from the surface photovoltage spectra using the procedure described in Ref.[36]. The equilibrium value of the surface band bending was the difference between the Fermi level position and the conduction band minimum. Fermi level position was obtained by a Fermi function fit to the low-energy shoulder of the surface charge density peak.

It is important to note that surface charge density spectra, while visually similar in overall shape to luminescence spectra, differ in several key aspects. First, they represent either occupied or unoccupied states exclusively, whereas luminescence spectra typically display all states together without distinguishing between them. Second, surface charge density spectra are quantitative, providing precise measurements of surface charge, whereas luminescence spectra are generally not suitable for such quantification. Third, the peaks in surface charge spectra are polar—either positive or negative—depending on the nature of the transition, involving the conduction or valence band, respectively. In this work, the peaks are positive. In contrast, luminescence peaks lack polarity and do not indicate the specific band involved in the transition.

X-ray photoelectron spectroscopy (XPS) analyses were conducted under ultra-high vacuum conditions (3×10^{-10} Torr) using a Thermo Fischer Scientific ESCALAB 250 Multitechnique System (USA), equipped with a double-focusing 180° spherical sector analyzer and a monochromatized Ag Lα radiation source (hν = 2984.3 eV). Measurements were performed at a pass energy of 117 eV with an energy step interval of 0.125 eV. Photoelectron spectra were collected from a spot with a diameter of 900 µm, maintaining a constant acquisition time across all experiments. Spectra were calibrated relative to a carbon 1s peak positioned at 284.8 eV to correct for charging effects.

Results

To probe the reversibility of surface charge modulation, we first removed charge from the GaN yellow band surface state by mild vacuum annealing (180 °C)[14]. Subsequent sequential exposure to H_2O, NO_2, and CO restored charge within the yellow band, with NO_2 uniquely reinstating the original charge distribution peak. This highlights NO_2 as the dominant atmospheric species interacting with the yellow band surface state and modulating its electronic properties.

We further examined whether H_2O and CO, like NO_2, interact with the yellow band surface state, producing distinct charge distribution peaks. Optical discharge experiments have already revealed that the Fermi level at the surface is governed by the charge associated with the yellow band, and that removal of this charge unpins the Fermi level in a Pt Schottky barrier[37]. The presently observed charge distribution peaks (Fig. 1) appear within the yellow band energy range but span only a portion of its expected distribution. This partial occupation suggests that the yellow band surface states are divided by the surface Fermi level: states below it are filled with charge, while those above remain unoccupied. Consequently, the low-energy shoulder of each peak is expected to exhibit a step-like profile defined by the Fermi function, which separates the charged and uncharged regions within the distribution. However, this step is broadened towards lower energies by the Franz–Keldysh effect, a result of the strong electric field inherent to the space charge region—peaking at the surface[38]. Despite this smearing, the Fermi level resulting from the adsorption of each of the three molecules can still be estimated. While it is theoretically possible to adjust the Fermi function to account for the Franz–Keldysh effect, doing so would require prior knowledge of both the Fermi level position and the surface electric field.

An example of the Fermi function placement on the spectral distribution of charge for NO_2 exposure is depicted in the inset of (Fig. 1). A similar fitting procedure was applied to each of the spectra for the different molecules, resulting in values of $E_C - E_F = 2.0, 2.27, and 2.41 eV$ for NO_2, H_2O, and CO, respectively. These values are plotted against the molecules' ionization energies in (Fig. 2). Since NO_2 appears to undergo cleavage—likely leaving the NO fragment attached to the surface—we plotted two points: one for NO and another for NO_2. The difference in their ionization energies is minor, as seen in the figure. Similarly, for water, which we suspect releases one hydrogen atom before attaching to the surface, the deviations are less significant; overall, the points

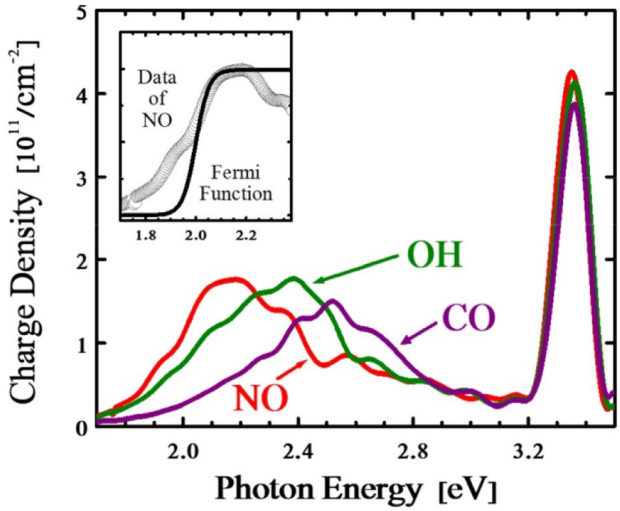

Fig. 1. Three charge density spectra were extracted from surface photovoltage measurements taken after mild heat treatment (170 °C) in vacuum, followed by exposure to one of three gases—NO_2, H_2O, or CO—leaked into the vacuum system. Each gas restored charge density within the yellow band, but produced a distinct peak in the corresponding energy range, with peak positions differing slightly among the gases. These differences are attributed here to variations in the surface Fermi level. To estimate the Fermi level position, we fit the low-energy shoulder of each peak using a Fermi function, as illustrated in the inset for the NO_2-induced peak. The left shoulder of each peak is broadened toward lower energies due to the Franz-Keldysh effect.

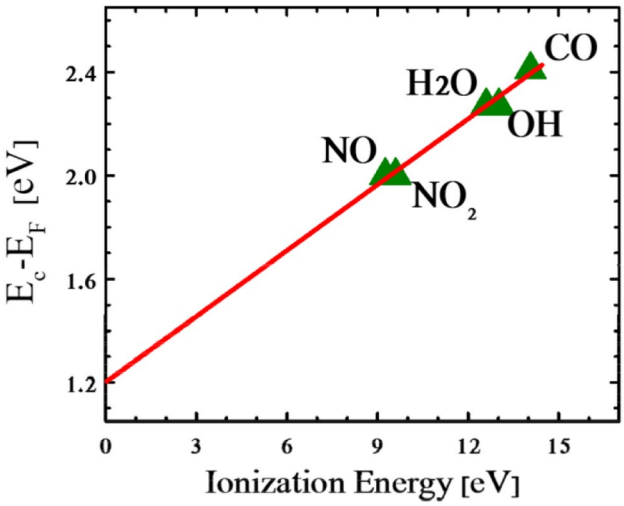

Fig. 2. The three Fermi level positions extracted from the peaks in (Fig. 1) are plotted against the ionization energies of the corresponding gases. For NO_2, we also include the ionization energy of NO, based on prior observations indicating that NO—not NO_2—is desorbed from the surface following NO_2 adsorption. This suggests that NO_2 undergoes cleavage upon adsorption. As shown, the ionization energy difference between NO and NO_2 is minimal. For H_2O, we also present the ionization energy of OH, although in this case, it remains unclear whether cleavage occurs. A linear fit through the three data points representing the gases is included.

tend to align along a straight line, indicating a linear relationship between the molecules' ionization energies and the resulting surface Fermi level positions. This linearity supports the hypothesis that the Ga-polar surface Fermi level is not pinned, but is tunable via molecular adsorption. The linear fit intersects the Fermi level energy axis at a point we denote as $E_C - E_{F0} = 1.2eV$, representing the Fermi level position in the absence of the adsorbed molecule. This value will be referenced later in the analysis.

Knowledge of the Fermi level positions allows for a fully quantitative calculation of the charge distribution spectrum for each molecule. As illustrated in Fig. 1, the spectra of all three molecules exhibit not only a dominant yellow band but also a minor blue band centered at 2.8 eV, which is attributed to Mg doping in the samples[39]. A sharp, narrow peak is also observed at the band edge.

The effect of molecular adsorption is contingent on the presence of the native Ga–O oxide layer. This dependence is evidenced by the observation that HCl etching of the surface, which removes the oxide, suppresses subsequent molecular adsorption effects. Figure 3 presents a comparison of the O 1s X-ray photoelectron spectroscopy (XPS) spectrum before and after etching, demonstrating the elimination of the Ga–O bond-associated component. Additionally, the etching process significantly reduces the charge density across the yellow band energy range, though a complete removal is not achieved, indicating some residual surface activity. (Fig. 4).

Table 1 summarizes the key parameters for each molecule: ionization energy, Fermi level position ($E_C - E_F$), band bending voltage (V_{BB}), and coverage density (N). Coverage density is reported both from peak area integration and from the electrostatic model described below.

Model and discussion

XPS analysis confirms that HCl etching effectively removes the native oxide, consistent with prior studies[40–43]. Distinct surface charge density peaks are observed only before etching, underscoring the critical role of the native oxide in enabling molecular adsorption and charge modulation.

On the Ga-face of GaN, a ~ 4 nm thick amorphous gallium oxide layer naturally forms, which is expected to be insulating[24,44,45]. Since ligand attachment occurs atop this oxide, the charge introduced by the ligand layer is analogous to the electrical biasing of a gate metal in a metal–oxide–semiconductor (MOS) capacitor.

Each adsorbed molecule produces a distinct charge density peak within the yellow band. We posit that these peaks are associated via their interaction with a shared surface state, an assertion substantiated by the data. Variations in the peak positions reflect shifts in the surface Fermi level. Since charge carriers can only occupy states below the Fermi level, its position must lie above the observed peaks, closer to the conduction band. This is consistent with the polarity of the photovoltage features, which indicate optical transitions from a deep acceptor level to the conduction band[36].

Figure 5 presents a surface state density modeled by a Gaussian distribution, which is bisected by a Fermi function. The portion at energies lower than the Fermi level represents unoccupied states, while the higher-energy portion corresponds to states filled with charge. The Fermi function itself marks the position of the Fermi level. The polarity of the surface photovoltage spectra indicates that the detected signal originates from the occupied states. Because the Fermi function sharply truncates the Gaussian distribution, the resulting charge density peak should exhibit a step-like profile on its low-energy side. However, real semiconductor surfaces often exhibit strong electric fields, which induce a smearing of this edge toward lower energies due to the Franz-

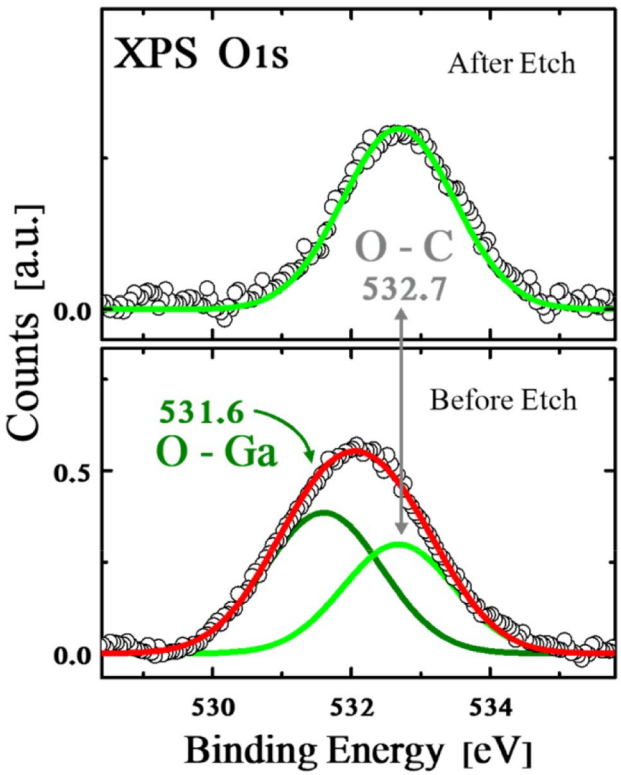

Fig. 3. X-ray photoelectron spectra (XPS) of the O 1 s binding energy range are shown before (bottom panel) and after (top panel) surface etching with HCl. The original spectrum consists of two distinct peaks: one at 531.6 eV, typically attributed to oxygen–gallium bonds, and another at 532.7 eV, commonly associated with oxygen–carbon bonds. Following etching, the oxygen–gallium peak is eliminated, while the oxygen–carbon peak remains unaffected.

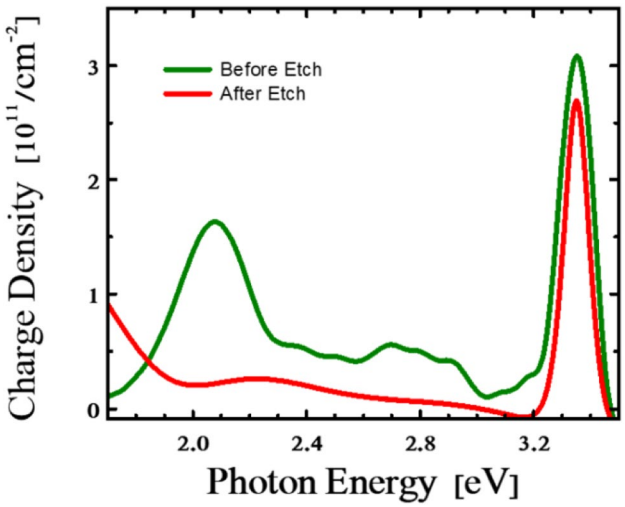

Fig. 4. Charge density spectra derived from surface photovoltage measurements taken before and after HCl surface etching reveal a reduction in surface charge density across the entire yellow band energy range, although the charge is not entirely eliminated.

Ligand type	Ionization energy	$E_C - E_F[eV]$	$V_{BB}[V]$	$N_{Calc}[10^{11}cm^{-2}]$	$N_{Meas}[10^{11}cm^{-2}]$
NO	9.26	2.0	1.85	1.49	1.17
NO_2	9.60				
OH	13.02	2.27	2.12	1.91	1.19
H_2O	12.6				
CO	14.07	2.41	2.26	2.12	0.92

Table 1. Summary of key parameters for each molecule, including ionization energy, Fermi level position ($E_C - E_F$), band bending voltage (V_{BB}), and surface coverage density (N). Coverage density is reported both from peak area integration and from model-based calculation.

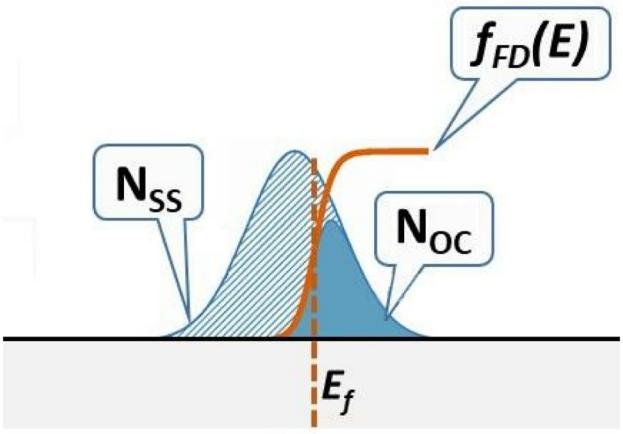

Fig. 5. A conceptual diagram of a surface state density (labeled N_{SS}), modeled here using a Gaussian distribution, is divided by the Fermi function. States at energies below the Fermi level (E_F) are unoccupied, while those above it are populated with charge carriers (labeled N_{OC}). The Fermi function defines the position of the Fermi level within the distribution.

Keldysh effect. Despite this broadening, fitting the data with a Fermi function remains feasible (as shown in the inset of Fig. 1). The energy position derived from such a fit, denoted E_{Fs}, represents the energy difference between the surface Fermi level and the conduction band minimum, E_C. By subtracting the bulk Fermi level, E_{FB}, also referenced to E_C, we obtain the surface band bending, V_{BB}:

$$qV_{BB} = E_{Fs} - E_{Fb} \tag{1}$$

Based on the carrier concentration in our samples ($N_D = 2 \cdot 10^{16} cm^{-3}$) and the intrinsic carrier concentration reported by Gachovska et al.[46] ($n_i = 1.9 \cdot 10^{-10} cm^{-3}$), the bulk Fermi level position is calculated to be $E_{FB} = 0.15eV$.

Results of the Fermi function fit for each of the three ligands are given along with the values of the surface band bending in (Table 1).

In MOS capacitor terminology, the concept most closely related to surface band bending at equilibrium is the "flat band voltage" (V_{FB}). This voltage corresponds to the difference between the work function of the gate metal—represented in our case by the ligand layer (ϕ_M)—and that of the semiconductor (ϕ_{SC}). An additional factor influencing V_{FB} is the voltage drop across charged interface states between the oxide and the semiconductor, expressed as Q_{SS}/C_{Ox}. Given that our semiconductor is n-type and the transferred charge to the ligands is assumed to be electrons, the flat band voltage represents the external voltage required to cancel the built-in potential and achieve flat energy bands. Consequently, it has the opposite sign of the built-in (band bending) voltage, such that $V_{BB} = -V_{FB}$. In our measurements, we directly determine the built-in voltage. Therefore

$$V_{BB} = \varnothing_M - \varnothing_{SC} + \frac{Q_{SS}}{C_{OX}} \tag{2}$$

The capacitance of the oxide is by far the weak part of this present model, because the typical thickness of the gallium oxide here is about 4 nm. This thickness along with the typical quality of this oxide form a "leaky" capacitor, which renders futile any attempt to calculate it using the common approach. We know it is "leaky", because the transfer of the charge between the ligands and the oxidized substrate must involve the native oxide. Nonetheless, the charges within the oxide must influence the band bending. Hence, Eq. (2) should be valid, even if the structure is one of a "bad" Schottky diode having an interfacial layer rather than a true MOS capacitor. Although not a conventional MOS device, the electrostatic treatment applies under equilibrium conditions. As there is no external gate voltage, there is no steady-state leakage current. So, while leakage prevents accurate capacitance extraction, the MOS analogy is still conceptually correct as far as the balance of potentials described in Eq. (2).

To calculate $\varnothing_{SC}$, we use an experimentally measured value of GaN affinity obtained from Lin et al.[47].

$$\varnothing_{SC} = \chi_{GaN} + E_{Fb} = 3.8 + 0.15 = 3.95eV$$

While Q_{SS} is unknown, it is buried either within or under the oxide and may be assumed to be fixed and not change, when we change the ligand. Q_{SS} also includes, in the case of GaN, the polar charge, which is definitely a fixed quantity. An estimation of Q_{SS} may be straightforwardly obtained from the linear fit of the three points in (Fig. 2). The fit intersects the y-axis at $1.2eV$ and therefore yields $V_{BB0} = 1.2eV - 0.15eV = 1.05eV$. We denote this point V_{BB0}, because at this special point the work function of the "metal" is nullified, and hence, from Eq. (2) we get

$$\varnothing_M = V_{BB} - 1.05 \tag{3}$$

The striking outcome of Eq. (3) is that all calculated work function values converge around approximately 1 eV. While ionization energy is the property of a single molecule, work function is a property of a layer. It is typically much lower than the ionization energy, but the difference rarely reaches the present extreme, unless we are observing a mechanism similar to that underlying the so-called *effectively negative electron affinity*[48]. Essentially, the molecules here are all sub monolayer oxides and are thus reminiscent of the case of the sub monolayer of Cs-O commonly used to induce negative electron affinity on the surface of, e.g., GaAs[49]. A practical photocathode would, of course, require a p-type substrate while in our case, it is an n-type, but the revealed effect of these three oxide ligands appears to be similar to that of the Cs-O dipole layer (for a conceptual band diagram, please see Fig. 6). However, here, there appear to be several added advantages to the use of, e.g., water molecules, instead of Cs-O. The H_2O, or OH, molecules are rather stable compared with the Cs-O, and unlike the Cs-O that is only physisorbed, these molecules appear to bond to the native oxide, and therefore, should yield a robust combination that may alleviate the vacuum requirement, as opposed to the case of Cs-O photocathodes. The disadvantage may be the need to tunnel through the native oxide which appears to be an essential part of the structure.

To confirm sub-monolayer coverage, we attempt to assess the density of the coverage for each of the molecules.

Allegedly, we could use the MOS model to this end. The difference between the work functions of our "metal" (ligand layer) and the work function of the semiconductor is such that on contact, the charge density exchanged is the product of the work function difference and the capacitance of the oxide. However, because the capacitor is "leaky", its value is, in practice, much lower than the one we could calculate. This significantly undermines the reliability of using the MOS model to estimate the density of adsorbed molecules.

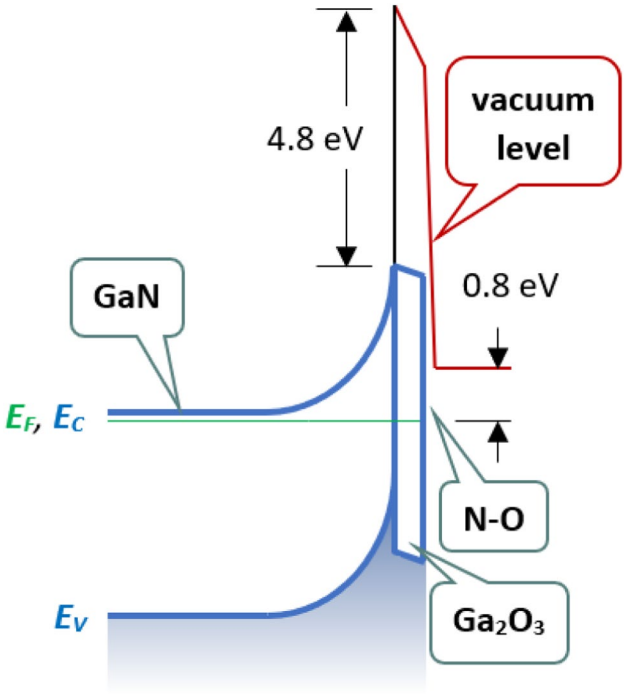

Fig. 6. A conceptual band diagram illustrating the surface arrangement of substrate, native oxide, and ligand layer. While the bandgap of the ligand and the electron affinity of the native oxide are not precisely known—and the latter remains somewhat speculative—the work function difference is established. If the molecules attach to the native oxide on a p-type substrate, the resulting structure may exhibit what is known as effective negative electron affinity.

Instead, the charge density added by the ligands may be calculated directly from the change it induces in the band bending (the following expression is derived from the solution to the Poisson equation and charge neutrality – see Section VII for detailed derivation)[50]:

$$N = \sqrt{\frac{2\varepsilon N_D}{q} V_{BB}} - \sqrt{\frac{2\varepsilon N_D}{q} V_{BB0}} \tag{4}$$

To obtain a certain validation to the values calculated using Eq. (4), we compare them (values given in Table 1) with the values obtained from the integrated area under the peaks in (Fig. 1). The results appear close enough to confirm the validity of our assumptions. This confirms that the peaks related to the ligands indeed set the position of the surface Fermi level. In fact, the actual differences between the charge densities above may be somewhat greater, because the value measured by integration includes charge from the slightly overlapping blue band. However, it makes perfect sense that the measured charge will be smaller than the real charge because the illumination never fully discharges the distribution. While in wide-gap materials it is easy to get close to a full discharge, because of the immense surface potential barrier that charges encounter on their way back to the surface trap, it is very difficult to reach a full discharge. The differences may also reflect errors in the positioning of the Fermi function.

Ultimately, the question remains: what is the precise structure of the adsorbate? For CO, the answer is straightforward—the adsorbed species appears to be chemically identical to the CO gas molecules introduced to the surface. In contrast, desorption experiments with NO_2 indicate that the desorbed species is NO, not NO_2. This suggests that NO_2 undergoes dissociation upon adsorption, with only NO remaining bound to the surface.

The case of H_2O is less clear. Due to this uncertainty, Fig. 2 presents ionization energies for all plausible species. The differences between NO_2 and NO, as well as between H_2O and OH, are relatively minor and do not significantly affect the interpretation of (Fig. 2). However, the observed low work function values point toward a dipole-like structure reminiscent of the Cs–O system—specifically, an O–x configuration, where x may be H, N, or C.

Given the current data, a definitive conclusion as to the exact nature of the adsorbate structure cannot be drawn, and therefore it remains an open question for future investigation.

Conclusion

This study presents compelling evidence that the surface electronic properties of GaN, particularly the position of the surface Fermi level, can be modulated by the ionization energy of adsorbed molecular species. Through surface photovoltage spectroscopy and x-ray photoelectron spectroscopy analysis, we demonstrate a linear

correlation between molecular ionization energy and Fermi level position, suggesting that the Ga-polar surface of GaN is not intrinsically pinned by bulk surface states. Instead, the modulation arises from charge transfer interactions mediated by the native oxide layer.

Our findings reveal that the native Ga–O oxide plays a pivotal role in enabling molecular adsorption and subsequent electronic modulation. Removal of this oxide layer suppresses the charge density peaks associated with adsorbed molecules, indicating that the active surface state resides at the GaN/native oxide interface rather than within the GaN bulk. This challenges conventional assumptions and highlights the importance of oxide–semiconductor interface engineering.

The observed low work function values of the ligand layers, significantly lower than their ionization energies, suggest the formation of dipolar structures akin to those found in Cs–O systems used for negative electron affinity surfaces. Unlike Cs–O, however, the molecular ligands studied here—such as H_2O, CO, and NO—form chemically bonded, stable configurations with the native oxide, potentially offering more robust and ambient-compatible alternatives for surface passivation and electronic tuning.

Outlook and practical implications

Our findings establish a framework for GaN surface engineering that leverages the linear relationship between adsorbate ionization energy and surface Fermi level position. This framework can be applied in several practical ways:

Device design and threshold control

By selecting molecular species or engineered dipolar layers with tailored ionization energies, designers can predictably modulate the surface Fermi level. This enables fine-tuning of threshold voltage, gate leakage, and current collapse in GaN-based HEMTs and MOSFETs without altering the bulk doping profile. Such control could complement or reduce reliance on complex epitaxial structures.

Passivation strategies

The study highlights the critical role of the native oxide in mediating charge transfer. This insight informs passivation layer design: rather than merely isolating the surface, passivation could be engineered to incorporate dipolar molecules or oxide chemistries that stabilize desired electronic states. This approach could mitigate reliability issues such as threshold drift and hot-electron degradation.

Reliability and encapsulation

While encapsulation and passivation typically shield the GaN surface from ambient molecules, the underlying mechanism remains relevant for long-term reliability. Interfaces formed during processing or under imperfect encapsulation can still interact with residual species. Understanding these interactions allows prediction of failure modes and guides the development of robust encapsulation schemes that preserve engineered surface states under thermal and electrical stress.

Advanced applications

The observed dipolar effects suggest opportunities beyond conventional electronics, such as negative electron affinity surfaces for photocathodes or sensors. These applications could exploit stable, oxide-bonded molecular layers as alternatives to fragile Cs–O systems, offering improved environmental stability.

Future directions

To translate these concepts into practical technologies, further research should focus on integrating controlled molecular layers during device fabrication and evaluating their stability under real-world conditions such as high temperature, bias stress, and packaging. In addition, exploring alternative oxide chemistries and a broader range of molecular species could enable more precise control of surface Fermi level positioning. Such efforts will not only advance passivation strategies but also open opportunities for novel functionalities, including negative electron affinity surfaces for optoelectronic applications. Ultimately, understanding the interplay between molecular dipoles, native oxides, and device reliability will be essential for bridging the gap between fundamental surface science and robust GaN-based electronics.

Charge density derivation

This section provides a comprehensive derivation of Eq. (4) presented in the main manuscript. The derivation begins with Poisson's equation for an n-type GaN surface under depletion, applies the depletion approximation, and uses charge neutrality to relate surface charge to band bending. Intermediate steps and assumptions are explicitly stated for clarity.

Step 1 *Start from Poisson's equation in one dimension for the semiconductor:*

$$\frac{d^2\psi}{dx^2} = -\frac{\rho}{\varepsilon_s}$$

Step 2 *Under the depletion approximation, the charge density is approximated as constant:*

$$\rho = -qN_D$$

for $0 < x < W$, where N_D is the donor concentration, q is the electronic charge, and W is the depletion width.

Step 3 *Integrating Poisson's equation twice gives the potential $\psi(x)$. At the surface ($x=0$), the band bending V_{BB} is related to W by:*

$$V_{BB} = \frac{qN_D W^2}{2\varepsilon_s}$$

Step 4 *The total charge in the depletion region is:*

$$Q_{dep} = qN_D W$$

Charge neutrality requires that this equals the trapped surface charge Q_s (with sign convention):

$$Q_s = -qN_D W$$

Step 5 *From Step 3, express W as:*

$$W = \sqrt{\frac{2\varepsilon_s V_{BB}}{qN_D}}$$

Substituting into Q_s gives:

$$Q_s = -\sqrt{2q\varepsilon_s N_D V_{BB}}$$

Step 6 *The change in surface charge when band bending changes from V_{BB0} to V_{BB} is*

$$\Delta Q_s = -\sqrt{2q\varepsilon_s N_D V_{BB}} + \sqrt{2q\varepsilon_s N_D V_{BB0}}$$

Dividing by the electron charge, q, gives the surface charge density difference. This is the expression presented as Eq. (4) in the manuscript.

Assumptions: Uniform doping, n-type GaN, one-sided junction, depletion approximation valid, and negligible inversion charge.

Data availability

Data will be made available on request from the corresponding author.

Received: 17 October 2025; Accepted: 6 January 2026
Published online: 14 January 2026

References

1. Cao, Y., Pomeroy, J. W., Uren, M. J., Yang, F. & Kuball, M. Electric field mapping of wide-bandgap semiconductor devices at a submicrometre resolution. *Nat. Electron.* **4**, 478. https://doi.org/10.1038/s41928-021-00599-5 (2021).
2. Huang, S. et al. Threshold voltage instability in III-nitride heterostructure metal–insulator–semiconductor high-electron-mobility transistors: Characterization and interface engineering. *Appl. Phys. Rev.* **11**, 021325. https://doi.org/10.1063/5.0179376 (2024).
3. Asubar, J. T., Yatabe, Z., Gregusova, D. & Hashizume, T. Controlling surface/interface states in GaN-based transistors: Surface model, insulated gate, and surface passivation. *J. Appl. Phys.* **129**, 121102. https://doi.org/10.1063/5.0039564 (2021).
4. Hashizume, T., Nishiguchi, K., Kaneki, S., Kuzmik, J. & Yatabe, Z. State of the art on gate insulation and surface passivation for GaN-based power HEMTs. *Mater. Sci. Semicon. Proces.* **78**, 85. https://doi.org/10.1016/j.mssp.2017.09.028 (2018).
5. Zeng, F. et al. A comprehensive review of recent progress on GaN high electron mobility transistors: Devices, fabrication and reliability. *Electronics* **7**, 377. https://doi.org/10.3390/electronics7120377 (2018).
6. Liu, C. et al. Effect of atmosphere on electrical characteristics of AlGaN/GaN HEMTs under hot-electron stress. *IEEE Trans. Electron. Dev.* **68**, 1000. https://doi.org/10.1109/TED.2021.3049764 (2021).
7. Kozak, J. P. et al. Stability, reliability, and robustness of GaN power devices: A review. *IEEE Trans. Pow. Electron.* **38**, 8442. https://doi.org/10.1109/TPEL.2023.3266365 (2023).
8. Deng, K. et al. Effective suppression of amorphous Ga 2O and related deep levels on the GaN surface by high-temperature remote plasma pretreatments in GaN-based metal–insulator–semiconductor electronic devices. *ACS Appl. Mater. Interfaces* **15**, 25058. https://doi.org/10.1021/acsami.3c03094 (2023).
9. Chen, J. et al. Formation and applications in electronic devices of lattice-aligned gallium oxynitride nanolayer on gallium nitride. *Adv. Mater.* **35**, 2208960. https://doi.org/10.1002/adma.202208960 (2023).
10. Mirrielees, K. J. et al. Native oxide reconstructions on AlN and GaN (0001) surfaces. *J. Appl. Phys.* **129**, 195304. https://doi.org/10.1063/5.0048820 (2021).
11. Maier, K. et al. Competitive adsorption of air constituents as observed on InGaN/GaN nano-optical probes. *Sens. Actuat. B Chem.* **250**, 91. https://doi.org/10.1016/j.snb.2017.04.098 (2017).
12. Li, Y. et al. Adsorption model for atoms and molecules on doped semiconducting oxides. *Phys. Rev. B* **109**, 195416. https://doi.org/10.1103/PhysRevB.109.195416 (2024).
13. Sato, M. et al. Comparative study of H2O and O2 adsorption on the GaN surface. *J. Phys. Chem. C* **125**, 25807. https://doi.org/10.1021/acs.jpcc.1c07110 (2021).
14. Turkulets, Y., Shauloff, N., Chaulker, O. H., Jelinek, R. & Shalish, I. Physics and chemistry of nitrogen dioxide (NO2) adsorption on gallium nitride (GaN) surface and its interaction with the yellow-luminescence-associated surface state. *J. Coll. Inter. Sci.* **678**, 789. https://doi.org/10.1016/j.jcis.2024.09.033 (2025).
15. Ryan, P. et al. Surface electronic structure of p-type GaN(000ī). *Surf. Sci.* **467**, L827 (2000).
16. Dong, Y., Feenstra, R. M. & Northrup, J. E. Oxidized GaN(0001) surfaces studied by Scanning tunneling microscopy and spectroscopy and by first-principles theory. *J. Vac. Sci. Technol. B* **24**, 2080. https://doi.org/10.1116/1.2214713 (2006).
17. Van de Walle, C. G. & Segev, D. Microscopic origins of surface states on nitride surfaces. *J. Appl. Phys.* **101**, 081704. https://doi.org/10.1063/1.2722731 (2007).

18. Himmerlich, M. et al. GaN(0001) surface states: Experimental and theoretical fingerprints to identify surface reconstructions. *Phys. Rev. B* **88**, 125304. https://doi.org/10.1103/PhysRevB.88.125304 (2013).
19. Shiozaki, N., Sato, T. & Hashizume, T. Formation of thin native oxide layer on n-GaN by electrochemical process in mixed solution with glycol and water. *Jap. J. Appl. Phys.* **46**, 1471. https://doi.org/10.1143/JJAP.46.1471 (2007).
20. Oon, H. S. & Cheong, K. Y. Recent development of gallium oxide thin film on GaN. *Mater. Sci. Semicon. Proc.* **16**, 1217. https://doi.org/10.1016/j.mssp.2013.01.027 (2013).
21. Irokawa, Y. et al. Electron microscopy and ultraviolet photoemission spectroscopy studies of native oxides on GaN(0001). *Jpn. J. Appl. Phys.* **57**, 098003. https://doi.org/10.7567/JJAP.57.098003 (2018).
22. Janicki, Ł et al. Thermal oxidation of [0001] GaN in water vapor compared with dry and wet oxidation: Oxide properties and impact on GaN. *Appl. Surf. Sci.* **598**, 153872. https://doi.org/10.1016/j.apsusc.2022.153872 (2022).
23. Shiojima, K. et al. Effect of surface treatment of printed Ag Schottky contacts on n-GaN epitaxial layers using Ag nanoink: Two dimensional characterization by scanning internal photoemission microscopy. *Jpn. J. Appl. Phys.* **57**, 07MA01. https://doi.org/10.7567/JJAP.57.07MA01 (2018).
24. Guo, J. et al. Effect of native oxide layer on mechanochemical reaction at the GaN-Al2O3 Interface. *Front. Chem.* **9**, 672240. https://doi.org/10.3389/fchem.2021.672240 (2021).
25. Chugh, M. & Ranganathan, M. Adsorbate interactions on the GaN(0001) surface and their effect on diffusion barriers and growth morphology. *Phys. Chem. Chem Phys.* **19**, 2111–2123. https://doi.org/10.1039/C6CP07254B (2017).
26. Ohuchi, Y., Saeki, H., Sakakima, H. & Izumi, S. Surface oxidation of GaN(0001) simulated by charge-transfer-type molecular dynamics. *Phys. Stat. Sol. B* **261**, 2400030. https://doi.org/10.1002/pssb.202400030 (2024).
27. Feenstra, R. M., Northrup, J. E. & Neugebauer, J. Review of structure of bare and adsorbate-covered GaN(0001) surfaces. *MRS Internet J. Nitride Semicond. Res.* **7**, 2002. https://doi.org/10.1557/S1092578300000296 (2014).
28. Pearce, B. L., Wilkins, S. J., Paskova, T. & Ivanisevic, A. A review of in situ surface functionalization of gallium nitride via beaker wet chemistry. *J. Mater. Res.* **30**, 2859. https://doi.org/10.1557/jmr.2015.132 (2015).
29. Auzelle, T. et al. Electronic properties of air-exposed GaN(11–00) and (0001) surfaces after several device processing compatible cleaning steps. *Appl. Surf. Sci.* **495**, 143514. https://doi.org/10.1016/j.apsusc.2019.07.256 (2019).
30. Liu, Z. et al. Predicting the catalytic activity of surface oxidation reactions by ionization energy. *CCS Chem.* **2**, 919–931 (2020).
31. Baumgarten, L. et al. Smart design of fermi level pinning in HfO2-based ferroelectric memories. *Ad. Func. Mater.* **34**, 2307120. https://doi.org/10.1002/adfm.202307120 (2024).
32. Liu, X., Choi, M. S., Hwang, E., Yoo, W. J. & Sun, J. Fermi level pinning dependent 2D semiconductor devices: Challenges and prospects. *Adv. Mater.* **34**, 2108425. https://doi.org/10.1002/adma.202108425 (2022).
33. Tachikawa, T., Minohara, M., Hikita, Y., Bell, C. & Hwang, H. Y. Tuning band alignment using interface dipoles at the Pt/Anatase TiO2 interface. *Adv. Mater.* **27**, 7458. https://doi.org/10.1002/adma.201503339 (2015).
34. Verdenhalven, E., Knorr, A., Richter, M., Bieniek, B. & Rinke, P. Theory of optical excitations in dipole-coupled hybrid molecule-semiconductor layers: Coupling of a molecular resonance to semiconductor continuum states. *Phys. Rev. B* **89**, 235314. https://doi.org/10.1103/PhysRevB.89.235314 (2014).
35. Futera, Z. & Blumberger, J. Electronic couplings for charge transfer across molecule/metal and molecule/semiconductor interfaces: Performance of the projector operator-based diabatization approach. *J. Phys. Chem. C* **121**, 19677. https://doi.org/10.1021/acs.jpcc.7b06566 (2017).
36. Turkulets, Y. et al. The GaN(0001) yellow-luminescence-related surface state and its interaction with air. *Surfaces Interfaces* **38**, 102834. https://doi.org/10.1016/j.surfin.2023.102834 (2023).
37. Shalish, I. et al. Yellow luminescence and Fermi level pinning in GaN films. *Appl. Phys. Lett.* **77**, 987. https://doi.org/10.1063/1.1288813 (2000).
38. Turkulets, Y. & Shalish, I. Franz-Keldysh effect in semiconductor built-in fields: Doping concentration and space charge region characterization. *J. Appl. Phys.* **124**, 075102. https://doi.org/10.1063/1.5038800 (2018).
39. Chaulker, O. H., Turkulets, Y. & Shalish, I. The Mg related GaN blue luminescence deep level and its connection to an MgO surface state. *Sci. Rep.* **15**, 18773. https://doi.org/10.1038/s41598-025-97446-w (2025).
40. Shalish, I., Shapira, Y., Burstein, L. & Salzman, J. Surface states and surface oxide in GaN layers. *J. Appl. Phys.* **89**, 390. https://doi.org/10.1063/1.1330553 (2001).
41. Tripathy, S., Chua, S. J. & Ramam, A. Electronic and vibronic properties of n-type GaN: the influence of etching and annealing. *J. Phys. Cond. Matt.* **14**, 4461. https://doi.org/10.1088/0953-8984/14/17/317 (2002).
42. Diale, M., Auret, F. D., van der Berg, N. G., Odendaal, R. Q. & Roos, W. D. Analysis of GaN cleaning procedures. *Appl. Surf. Sci.* **246**, 279. https://doi.org/10.1016/j.apsusc.2004.11.024 (2005).
43. Winner, A., Garrido, J. A. & Stutzmann, M. GaN surface states investigated by electrochemical studies. *Appl. Phys. Lett.* **110**, 101602. https://doi.org/10.1063/1.4977947 (2017).
44. Dycus, J. H. et al. Structure of ultrathin native oxides on III–nitride surfaces. *ACS Appl. Mater. Interfaces* **10**, 10607. https://doi.org/10.1021/acsami.8b00845 (2018).
45. Hossain, T. et al. Insulating gallium oxide layer produced by thermal oxidation of gallium-polar GaN. *Phys. Stat. Sol. C.* **11**, 565. https://doi.org/10.1002/pssc.201300659 (2014).
46. Gachovska, T. K. & Hudgins, J. L. SiC and GaN power semiconductor devices. In *Power Electronics Handbook* (ed. Rashid, M. H.) (Butterworth-Heinemann, 2018).
47. Lin, S. C. et al. Experimental determination of electron affinities for InN and GaN polar surfaces. *Appl. Phys. Express* **5**, 031003. https://doi.org/10.1143/APEX.5.031003 (2012).
48. Wang, X. et al. Negative electron affinity of the GaN photocathode: a review on the basic theory, structure design, fabrication, and performance characterization. *J. Mater. Chem. C* **9**, 13013. https://doi.org/10.1039/D1TC03244E (2021).
49. Liu, L., Diao, Y. & Xia, S. Impact of gas adsorption on the stability and electronic properties of negative electron affinity GaAs nanowire photocathodes. *J. Coll. Interface Sci.* **572**, 297. https://doi.org/10.1016/j.jcis.2020.03.100 (2020).
50. Sze, S. M. & Ng, K. K. *Physics of Semiconductor Devices* (John Wiley & Sons, 2007).

Acknowledgements

We acknowledge the Ilse Katz Institute for Nanoscale Science & Technology at Ben Gurion University and Michigan Center for Materials Characterization for use of the instruments and staff assistance.

Author contributions

Conceptualization, I.S.; methodology, I.S. and Y.T.; experimentation, O.H.C and Y.T.; formal analysis, I.S.; writing—original draft preparation, I.S.; writing—review and editing, O.H.C., Y.T., Y.S., R.S.G., and I.S.; funding acquisition, I.S. and R.S.G. All authors have read and agreed to the published version of the manuscript.

Funding

We gratefully acknowledge the support of BSF grant #2022627, NSF grant # ECCS- 2240388, and the Office

of Naval Research Global through a NICOP Research Grant (No. N62909-26-1-2000). The views expressed are those of the author and do not reflect the official policy or position of the Department of War or the U.S. Government. DISTRIBUTION STATEMENT A. Approved for public release: distribution is unlimited. DCN# 2025-10-22-1607.

Declarations

Competing interests
The authors declare no competing interests.

Additional information
Correspondence and requests for materials should be addressed to I.S.

Reprints and permissions information is available at www.nature.com/reprints.

Publisher's note Springer Nature remains neutral with regard to jurisdictional claims in published maps and institutional affiliations.